Secure Systems Design and Technology Development. Veliko Tarnovo, Bulgaria
Proceedings of the International Scientific Conference, 2026. Volume III, 379-386

Secure and Resilient Operation of Hybrid PV-Wind-Storage Systems for Modular E-Fuel Production under Disturbances

Iliyan Hutov
Defence Institute
"Professor Tsvetan Lazarov"
Sofia, Bulgaria
i.hutov@di.mod.bg

Petia Nedyalkova
Defence Institute
"Professor Tsvetan Lazarov"
Sofia, Bulgaria
https://orcid.org/0009-0006-7156-0891

Hristo Hristov
Defence Institute
"Professor Tsvetan Lazarov"
Sofia, Bulgaria
h.hristov@di.mod.bg

***Abstract*—Secure and resilient operation is a critical requirement for modular Power-to-Liquid e-fuel plants supplied by intermittent renewable energy. This paper investigates a modular e-fuel production architecture powered by a hybrid photovoltaic-wind-battery system and evaluates its response to short-duration renewable disturbances. A deterministic operational model is formulated for renewable generation, battery buffering, electrolyzer dispatch, hydrogen production, and aggregate fuel synthesis. To improve engineering realism, the framework incorporates electrolyzer ramp-rate constraints and a degradation-aware operating index. The optimization objective is to sustain fuel continuity while limiting curtailment, electrolyzer power variance, and dynamic stress. Beyond the main stressed-case comparison, the study includes sensitivity analysis of the PV/Wind ratio and storage capacity, together with Monte Carlo uncertainty analysis under stochastic renewable fluctuations. Relative to the no-buffer baseline, the optimized dispatch increases daily fuel output by 11.6%, reduces electrolyzer power variance by 66.3%, and improves the disturbance-window resilience score by 36.2%. The results show that secure operation of modular PtL plants emerges from coordinated design of renewable mix, storage, and supervisory control rather than from renewable-following logic alone.**

Keywords*—*deterministic optimization, hybrid PV-wind-storage system, modular e-fuel production, resilient operation.

I. INTRODUCTION

Power-to-Liquid (PtL) technology is increasingly regarded as a practical pathway for producing low-carbon synthetic fuels for aviation, maritime transport, and other hard-to-electrify sectors [4], [10]–[12]. Yet the viability of modular e-fuel plants depends not only on the nominal efficiency of chemical conversion, but also on the secure and resilient operation of the upstream energy-supply system. In hybrid renewable architectures, photovoltaic generation, wind generation, battery storage, and electrolyzer dispatch are strongly coupled in time, so renewable intermittency can propagate into instability, curtailment, reduced fuel continuity, and increased component stress [9], [13]–[15].

This challenge is especially relevant for modular industrial concepts inspired by current INERATEC-type deployments, where plant operation must remain robust under fluctuating renewable input and short-duration disturbances [2], [3]. In such systems, operational security is not a peripheral issue; it is a systems-design problem. Resilience, system stability, and disturbance handling must therefore be treated as explicit engineering objectives rather than secondary performance outcomes [1], [9].

Against this background, the present paper studies the secure and resilient operation of a hybrid PV-wind-storage system supplying a modular e-fuel plant under disturbances. The contribution is fourfold. First, it formulates a deterministic plant-operation model and the associated supervisory optimization problem. Second, it quantifies the operational benefit of the optimized strategy using explicit performance metrics. Third, it evaluates design sensitivity with respect to the PV/Wind ratio and storage capacity, and tests robustness through Monte Carlo uncertainty analysis. Fourth, it adds engineering realism by introducing electrolyzer ramp-rate constraints and a compact degradation-aware operating model. Throughout the manuscript, industrial ERA ONE values are treated as literature-reported benchmark data, while the fuel-output, resilience, curtailment, and degradation-related metrics are simulated or derived quantities generated by the reduced-order supervisory model. The resulting framework is

Online ISSN 3044-7771
https://doi.org/10.68302/std2026.vol3.180

closely aligned with the conference themes of secure systems design, system stability, disturbance handling, and sustainable energy technology development.

II. OPERATIONAL FRAMING FOR SECURE AND RESILIENT PTL SYSTEMS

The target plant is represented by six coupled subsystems: photovoltaic generation, wind generation, battery storage, a proton-exchange-membrane electrolyzer, a hydrogen buffer, and an aggregate fuel-synthesis block. The scope is operational rather than reactor-level. The hydrogen buffer is included conceptually as an intermediate continuity element between electrolysis and aggregate fuel synthesis; in the present reduced-order formulation, it is not resolved by a full state-space mass-balance model and is therefore not assigned a separately optimized storage trajectory. Instead, its role is reflected indirectly through the continuity objective and the disturbance-resilience interpretation. The model does not attempt catalyst-scale chemistry or CFD; instead, it captures the cross-couplings that determine plant-level resilience, stability, and fuel output under intermittent renewable supply.

From an operational systems viewpoint, resilience is not a property of a single component. It emerges from the coordinated behavior of the photovoltaic, wind, storage, and electrolyzer subsystems during shortages and surpluses. In this study, system stability is represented by low electrolyzer-power variance and reduced dynamic stress, while disturbance handling is represented by output retention during a forced one-hour renewable shortfall. This framing keeps the paper closely aligned with secure systems design in its engineering sense.

III. OPERATIONAL MODEL AND DETERMINISTIC OPTIMIZATION

The operational simulation horizon is 24 h with a 5 min time step. Renewable input is generated from a daytime photovoltaic profile and a non-zero wind profile in order to represent the hybrid PV-wind supply of the modular plant. Because no site-specific measured renewable traces are used in the numerical examples, these profiles are treated as benchmark stress-test signals rather than as production forecasts. The same supervisory model is written so that measured SCADA data, meteorological measurements, or reanalysis-derived irradiance and wind-speed time series can replace the synthetic profiles without changing the control problem. In a measured-profile implementation, PV power should be computed from plane-of-array irradiance and module temperature, while wind power should be mapped from hub-height wind speed through the turbine power curve before applying the same battery, electrolyzer, and hydrogen-buffer constraints. The battery model includes both an energy-capacity constraint and symmetric charge/discharge power limits of 0.40 MW, which prevents unrealistically large short-term buffering actions. The aggregate renewable power before auxiliary-load subtraction is defined as follows:

$$P_{RES}(t) = P_{PV}(t) + P_W(t) \qquad (1)$$

where P_{RES} is the aggregate renewable power, P_{PV} and P_W are photovoltaic and wind power

After subtracting the auxiliary load, the remaining power can be directed to the electrolyzer, battery charging, or curtailment. With positive battery power defined as discharge, the power balance is

$$P_{RES}(t) + P_{BAT}(t) = P_{EL}(t) + P_{AUX} + P_{CURT}(t) \quad (2)$$

where P_{BAT} is battery power, P_{EL} is electrolyzer power, P_{AUX} is auxiliary load, P_{CURT} is curtailed power,

The battery state evolves according to a charge/discharge efficiency model, where SOC(t) is the battery state of charge at time step t, expressed as a normalized value or percentage of the rated battery capacity. SOC(t+1) is the battery state of charge at the next time step. $P_{CH}(t)$ is the battery charging power at time t, $P_{DIS}(t)$ is the battery discharging power at time t, η_{ch} is the charging efficiency, and η_{dis} is the discharging efficiency. Δt is the simulation time step, and E_{BAT} is the rated battery energy capacity.

$$SOC(t+1) = SOC(t) + \frac{\left[\eta_{ch} P_{CH}(t) - \frac{P_{DIS}(t)}{\eta_{dis}}\right]\Delta t}{E_{BAT}} \quad (3)$$

The first term inside the brackets increases the state of charge during charging, while the second term decreases the state of charge during discharging. The division by E_{BAT} converts the exchanged energy into a normalized change of battery state of charge.

Hydrogen production is approximated by a power-proportional relationship. At this supervisory level, the downstream fuel-synthesis block is intentionally aggregated rather than reactor-resolved where $\dot{m}_{H2}(t)$ is the hydrogen produced by the electrolyzer during time step t, η_{EL} is the electrolyzer efficiency, $P_{EL}(t)$ is the electrical power supplied to the electrolyzer at time t, Δt is the simulation time step, and LHV_{H2} is the lower heating value of hydrogen. The numerator $\eta_{EL}P_{EL}(t)\Delta t$ represents the useful energy converted into hydrogen, while division by LHV_{H2} converts this energy into an equivalent hydrogen mass.

$$\dot{m}_{H2}(t) = \frac{\eta_{EL} P_{EL(t)\Delta t}}{LHV_{H2}} \qquad (4)$$

and aggregate synthetic-fuel output is represented by a simplified conversion relationship. This mapping is used only to compare dispatch strategies under common assumptions and should not be interpreted as a detailed process model or direct plant-validation equation.

$$m_{FUEL}(t) = k_{FT} m_{H2}, FT(t) \qquad (5)$$

where $m_{FUEL}(t)$ denotes the synthetic-fuel mass produced during time step t, $m_{H2}, FT(t)$ is the hydrogen mass directed to the aggregate Fischer–Tropsch synthesis block, and k_{FT} is the simplified hydrogen-to-fuel conversion coefficient. This coefficient is used as a reduced-order representation of the downstream synthesis process and is intended for comparative dispatch analysis rather than detailed reactor-level modelling.

The deterministic supervisory objective penalizes renewable curtailment and aggressive stack motion, rewards smooth fuel production, and includes a normalized fuel-output term. Tildes denote normalized quantities used only for weighting and numerical conditioning where J denotes the supervisory optimization objective, P_{CURT} is the curtailed renewable power, ΔP_{EL} is the electrolyzer power change between consecutive time steps, m_{FUEL} is the produced synthetic-fuel mass, m_{REF} is the reference fuel-production trajectory, and w1-w4 are weighting coefficients. The first term penalizes renewable curtailment, the second term penalizes aggressive electrolyzer ramping, the third term penalizes deviation from the desired fuel-production trajectory, and the fourth term rewards total synthetic-fuel production:

$$J = w1\, \Sigma P_{CURT} + w2\, \Sigma(\Delta P_{EL})^2 + w3\, \Sigma(m_{FUEL} - m_{REF})^2 - w4\, \Sigma m_{FUEL} \quad (6)$$

The optimization is subject to the operating-envelope constraints, where u(t) is the electrolyzer on/off state and the battery energy and power remain within rated limits and $P_{EL}(t)$ denotes the electrolyzer power at time step t, *Pmin* and *Pmax* define the allowable electrolyzer operating range, SOC(t) is the normalized battery state of charge, and $P_{CURT}(t)$ is the curtailed renewable power. These constraints ensure that the electrolyzer remains within its stable operating envelope, the battery does not exceed its energy limits, and renewable curtailment is treated as a non-negative surplus-power variable:

$$Pmin \le P_{EL}(t) \le Pmax, 0 \le SOC(t) \le 1,\ P_{CURT}(t) \ge 0 \quad (7)$$

and, for engineering realism, an explicit ramp-rate limit

$$|P_{EL}(t) - P_{EL}(t-1)| \le Rmax\, \Delta t \quad (8)$$

where $P_{EL}(t)$ denotes the electrolyzer power at the current time step, $P_{EL}(t-1)$ is the electrolyzer power at the previous time step, $Rmax\, \Delta t$ is the maximum allowable ramp rate of the electrolyzer, and Δt is the simulation time step. This constraint prevents unrealistically fast set-point changes and keeps the electrolyzer trajectory compatible with stack and balance-of-plant dynamic limitations.

Equation (8) is important because, without it, a controller may exploit the battery as an ideal actuator and command unrealistic stack transitions. By enforcing a maximum set-point gradient, the dispatch remains more compatible with actual balance-of-plant hardware and stack dynamics, which is consistent with recent experimental and review-based evidence for dynamic water-electrolysis systems [5]–[8].

The optimization was implemented as a deterministic reduced-order supervisory-control problem solved over 288 time steps per day. The decision variables are the electrolyzer power trajectory $P_{EL}(t)$ and the battery charge/discharge schedule. The main constraints are the electrolyzer operating window, the battery state-of-charge bounds, the battery power limit, non-negative curtailment, and the electrolyzer ramp-rate limit. A constrained sequential quadratic programming routine was used in the reference implementation. The stopping rule was a relative objective-function change below 10^{-6} or a maximum of 200 iterations. For the nominal and stressed cases reported here, convergence was typically reached within 20–35 iterations, with wall-clock runtimes below 0.5 s per 24 h case on a standard laptop-class processor.

All objective-function terms were normalized before weighting in order to keep the optimization numerically well-conditioned and to make the design priorities explicit. Curtailment was normalized by a daily curtailment reference scale, the ramp-smoothness term by the baseline sum of squared power steps, the fuel-continuity term by the baseline deviation from the reference production trajectory, and the fuel-maximization term by baseline daily fuel output. Unless otherwise stated, the reported cases use unit weights after normalization for the comparative terms in (6); therefore, the weights represent scheduling priorities rather than physically measurable plant constants.

TABLE I. MAIN MODEL PARAMETERS AND OPERATING LIMITS

Item	Value/ definition	Role in the model
Decision variables	P_EL(t), battery charge/discharge schedule	Supervisory control trajectories
Time discretization	24 h horizon, 5 min step, 288 intervals	Deterministic operating horizon
Solver	Sequential quadratic programming	Constrained nonlinear optimization
Stopping rule	Relative objective change < 10^-6 or 200 iterations	Convergence criterion
Normalization	Curtailment, ramp term, continuity term, fuel term normalized before weighting	Numerical conditioning and priority balancing
Battery power limit	±0.40 MW	Prevents unrealistically large short-term buffering actions

Figure 1 shows the simulated renewable supply used in the study. It includes both surplus and shortage periods and is therefore sufficient to test storage behaviour and renewable curtailment within the assumed operational scenario.

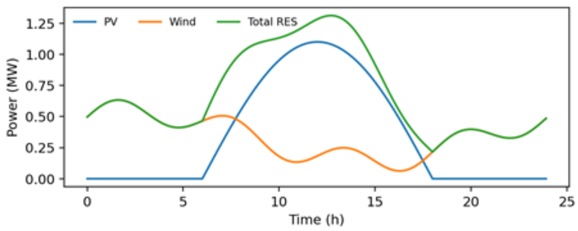

Fig. 1. Simulated 24 h renewable input for the reference case.

The profile contains both surplus and deficit periods and therefore provides an assumed, but stress-relevant test signal for battery buffering and curtailment behavior.

The mathematical formulation combines standard reduced-order models for battery state-of-charge evolution, electrolyzer hydrogen production, fuel-output aggregation, operational constraints, and ramp-rate limitation. These relationships are commonly used in energy-system and Power-to-X dispatch modelling. The paper does not claim novelty in the individual equations. Its methodological contribution is the integrated disturbance-aware supervisory formulation, including the combined objective function and the compact degradation-aware operating index used for comparative dispatch evaluation.

IV. SIMULATION SETUP AND DISTURBANCE SCENARIOS

The baseline case has no storage support and no dispatch optimization. It follows available renewable power subject to a minimum stable load and incurs cold-start penalties after reactivation. The optimized case adds battery buffering and deterministic smoothing with the ramp-rate limit. Two operating conditions are evaluated. The nominal case uses the synthetic renewable day without an imposed event. The stressed case introduces a one-hour renewable shortfall of 45% centered around noon. This event is not tied to a specific weather mechanism; rather, it serves as a clean disturbance-handling test. Such stress testing is appropriate for secure-systems-oriented evaluation because it isolates controller behavior under loss-of-supply conditions [1], [9].

The resilience score is defined as the ratio between mean electrolyzer power during the disturbance window and the pre-disturbance reference level. This keeps the resilience metric directly linked to process continuity. The main comparison is deliberately simple: a no-buffer baseline versus buffered optimized dispatch under the same renewable input. As a result, the reported percentage changes can be attributed to control and storage design rather than to a different resource profile.

The resilience score is adopted as the primary metric because it directly quantifies process continuity during the disturbance window and can be compared consistently across scenarios. It is intentionally narrow and is therefore complemented by uncertainty indicators, lower-tail production behaviour, and degradation trends. Additional resilience indicators that could be introduced in future work include minimum electrolyzer power during the disturbance, recovery time after disturbance, cumulative production loss, hydrogen-buffer depletion risk, and the number of operating-threshold violations.

V. RESULTS: SYSTEM STABILITY, RESILIENCE, AND DISTURBANCE HANDLING

Figure 2 compares electrolyzer dispatch during the stressed case. The baseline controller follows the renewable shortfall directly, whereas the optimized controller uses battery support and ramp shaping to maintain a flatter trajectory. This directly improves system stability because the power signal becomes less oscillatory. It also improves disturbance handling because the power level in the shortfall window is better preserved.

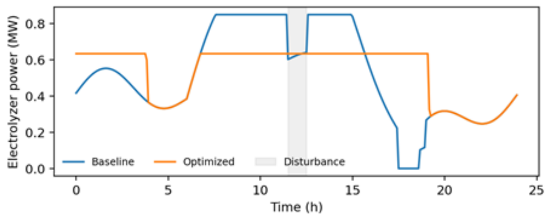

Fig. 2. Electrolyzer power during a forced one-hour renewable disturbance.

The optimized trajectory is flatter, which indicates better disturbance ride-through and lower dynamic stress.

The fuel effect follows the same pattern. Figure 3 shows cumulative daily fuel output. The optimized trajectory remains above the baseline because part of the renewable surplus is shifted through the battery instead of being wasted, and because the electrolyzer avoids repeated unstable operation around the minimum-load threshold. The reported fuel-output values should be interpreted as simulated control-oriented production indicators derived from an intentionally aggregated conversion model, not as plant-validated process-production estimates.

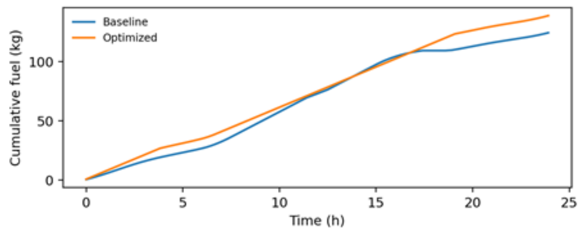

Fig. 3. Cumulative synthetic-fuel output in the stressed case.

The optimized trajectory remains above the baseline throughout the day, indicating improved fuel continuity.

The quantified results confirm the operational value of the proposed strategy within the reduced-order supervisory model. Under the stressed case, the optimized dispatch increases simulated daily fuel production by 11.6%, lowers electrolyzer-power variance by 66.3%, and improves the disturbance-window resilience score by 36.2%. These values should therefore be interpreted as model-derived indicators of dispatch quality under common assumptions, not as experimentally validated plant-scale production guarantees.

TABLE II. MAIN PERFORMANCE METRICS FOR THE STRESSED OPERATING CASE

Metric	Baseline	Optimized	Change
Daily fuel output (kg/day)	124.3	138.7	+11.6%
Electrolyzer power variance (-)	0.0646	0.0217	-66.3%
Resilience score (-)	0.734	1.000	+36.2%

VI. SENSITIVITY AND UNCERTAINTY ANALYSIS OF HYBRID OPERATION

Sensitivity analysis was added along two reviewer-critical axes: renewable-mix selection and storage sizing. The total installed renewable capacity was kept constant while the PV/Wind ratio was varied, and battery capacity was swept from 0.0 MWh to 1.6 MWh. These two variables strongly influence curtailment, stability, and degradation accumulation.

TABLE III. SENSITIVITY ANALYSIS WITH RESPECT TO PV/WIND RATIO

PV/Wind ratio	Fuel output (kg/day)	Curtailment (MWh/day)	Degradation index (-)	Interpretation
70/30	96.1	5.05	7.10	Solar-heavy, noon peaking
50/50	134.9	1.82	4.28	Balanced mix
30/70	151.9	0.63	3.99	Wind-heavier, best resilience

The renewable-mix sweep shows that a PV-dominant design concentrates power around midday and therefore increases curtailment and dynamic stress. A more balanced or wind-heavier mix extends useful generation into non-daylight periods and reduces the burden on storage. In this study, the wind-heavier 30/70 PV/Wind split yields the highest fuel output, while the 50/50 case offers the most balanced engineering compromise. This trend is consistent with the literature on complementarity in hybrid renewable systems and storage-assisted dispatch [9], [13], [15].

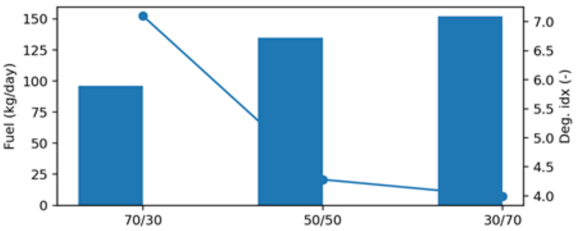

Fig. 4. Renewable-mix sensitivity results for constant total installed renewable capacity.

A more balanced or wind-heavier mix extends useful generation into non-daylight periods and reduces the burden on storage. In this study, the wind-heavier 30/70 PV/Wind split yields the highest simulated fuel output, while the 50/50 case offers the most balanced engineering compromise.

TABLE IV. SENSITIVITY ANALYSIS WITH RESPECT TO BATTERY ENERGY CAPACITY

Battery energy capacity (MWh)	Fuel output (kg/day)	Curtailment (MWh/day)	Degradation index (-)	Resilience score (-)
0.0	117.9	3.07	4.40	0.983
0.4	124.2	2.63	4.30	1.000
0.8	131.7	2.08	4.29	1.000
1.2	138.7	1.58	1.21	1.000
1.6	144.8	1.16	1.15	1.000

Moderate storage captures most of the modeled continuity benefit, while additional capacity above about 1.2 MWh yields diminishing returns.

To add uncertainty analysis, a Monte Carlo ensemble of 300 synthetic days was generated by perturbing hourly photovoltaic and wind amplitudes. The photovoltaic perturbation used an 18% standard deviation and the wind perturbation a 12% standard deviation. These values are not intended as site-specific forecast-error statistics; they are deliberately chosen stress-test amplitudes that create substantial but plausible renewable variability around the deterministic profile. Hourly multipliers were sampled from truncated normal distributions, clipped to avoid negative generation, and linearly interpolated to the 5 min simulation grid. PV and wind perturbations were treated as independent in the present study, which is a simplifying assumption and a clear target for future work with measured site data and temporally correlated forecast errors. This uncertainty envelope tests controller robustness rather than providing a probabilistic production forecast [1], [9].

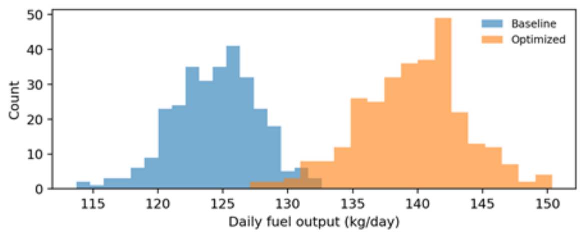

Fig. 5. Monte Carlo distribution of daily fuel output under renewable uncertainty.

The optimized distribution is shifted upward and narrower than the baseline distribution, indicating stronger robustness.

TABLE V. MONTE CARLO UNCERTAINTY SUMMARY FOR DAILY FUEL OUTPUT

Metric	Baseline	Optimized
Mean fuel output (kg/day)	124.5	139.6
5th percentile (kg/day)	119.0	132.4
Prob. fuel <125 kg/day	0.54	0.00

The uncertainty results confirm that the optimized strategy remains preferable across a distribution of renewable days. It improves the ensemble mean and, more importantly, the lower-tail behavior: the 5th-percentile daily fuel output is substantially higher, and the probability of dropping below 125 kg/day is reduced to zero in the simulated ensemble. These Monte Carlo outputs remain model-derived operational indicators rather than experimentally validated plant-throughput measurements.

VII. DEGRADATION-AWARE OPERATION

Engineering realism is increased further by making degradation an explicit scheduling concern. A compact degradation-aware index is introduced for dispatch comparison:

$$D(t+1) = D(t) + \alpha|\Delta P_{EL}(t)| + \beta N_{SS}(t) + \gamma u_{over}(t) \qquad (9)$$

where D(t) denotes the accumulated degradation-aware operating index at time step t, $\Delta P_{EL}(t)$ is the electrolyzer power change, $N_{SS}(t)$ is the start-stop event indicator or count, and $\gamma u_{over}(t)$ represents near-limit or over-operation. The coefficients α, β, and γ weight the contributions of ramp-induced stress, start-stop stress, and near-limit operating stress, respectively. The index is used as a comparative dispatch-level stress indicator rather than as a calibrated lifetime prediction model.

The first term penalizes ramp-induced stress, the second term penalizes start-stop events, and the third term penalizes sustained near-limit operation through

$$L_{high}(t) = \max\left[0, \frac{P_{EL}(t) - P_{high}}{P_{ELmax}, - P_{high}}\right] \tag{10}$$

where $L_{high}(t)$ denotes the normalized high-load operation indicator at time step t, $P_{EL}(t)$is the electrolyzer power, P_{high} is the threshold above which operation is treated as high-load operation, and P_{ELmax} is the maximum allowable electrolyzer power. The maximum operator ensures that the indicator remains zero below the high-load threshold and increases toward unity as the electrolyzer approaches its maximum operating power.

For the normalized comparisons reported here, α = β = γ = 1 after scaling each term to the same order of magnitude. This makes the index transparent and reproducible while avoiding the false precision of uncalibrated aging constants.

The degradation index should therefore be read as a comparative operating-stress indicator rather than a lifetime predictor. In the present study, lower degradation-index values coincide with smoother optimized dispatch in both the sensitivity analysis and the main-case results. A natural next step is to calibrate the three coefficients against stack-specific aging data, especially for PEM systems exposed to frequent renewable cycling [5], [8].

Industrial and literature-reported experimental benchmarks are used in this study to check consistency of scale and dynamic behaviour, not to claim direct model validation. These benchmarks help assess whether the assumed supervisory operating ranges remain industrially plausible, but they do not provide one-to-one validation of the reduced-order model because the latter intentionally aggregates synthesis dynamics and does not reproduce plant-specific thermal and mass-balance behaviour.

In addition to the simulation-based evaluation, real industrial and experimental benchmarks help interpret the operating assumptions used in this paper. According to INERATEC's official ERA ONE information, the Frankfurt-Höchst plant is being scaled to 7 MW and up to 2,500 t/year of sustainable e-Fuels, while recycling up to 8,000 t/year of CO2 [2], [3]. These values correspond to an average nominal fuel-production rate of approximately 285 kg/h, a specific fuel productivity of about 357 t/year per MW of installed plant capacity, and a CO2-to-fuel ratio of about 3.2 t/t. The purpose of these benchmark values is not to claim one-to-one validation of the reduced-order supervisory model, but to anchor the study in a realistic industrial scale and to show that modular PtL plants already operate at non-trivial process-throughput levels.

TABLE VI. INDUSTRIAL-SCALE BENCHMARK DATA DERIVED FROM ERA ONE

Metric	Value	Meaning / source
Installed PtL capacity	7 MW	Official ERA ONE plant scale [2], [3]
Annual e-fuel output	2,500 t/year	Official ERA ONE production target [2], [3]
Annual CO2 recycle	8,000 t/year	Official ERA ONE CO2 recycle target [2]
Average nominal fuel output	≈285 kg/h	Derived from 2,500 t/year / 8,760 h
Specific fuel productivity	≈357 t/year/MW	Derived from 2,500 t/year / 7 MW
CO2 per tonne of fuel	≈3.2 t/t	Derived from 8,000 / 2,500

Published experimental results for industrial alkaline electrolysis provide more direct support for the dynamic constraints adopted in the model. Gu et al. investigated a 250-kW alkaline system and reported three characteristic response scales: current-step responses in the order of seconds, hydrogen-in-oxygen and pressure dynamics in the order of minutes, and thermal start-stop dynamics in the order of hours [7]. Their variable-load test included transitions from full load at 3,500 A and 1.7 MPa to minimum-load operation at 1,400 A and 1.7 MPa, as well as a lower operating point of 800 A and 0.6 MPa [7]. These results are directly relevant for secure operation because they show that even when electrical response is fast, gas-purity, temperature, and pressure variables impose slower and safety-relevant limits on plant dispatch.

TABLE VII. LITERATURE-REPORTED EXPERIMENTAL RESULTS RELEVANT TO CONTROL DESIGN

Metric	Value	Meaning / source
Industrial electrolyzer test platform	250 kW alkaline system	Representative for 100-kW to MW-class systems [7]
Cold start sequence	25 °C to full load at 90 °C	Temperature-limited start-stop transition [7]
Hot shutdown / hot start	75 °C shutdown, 70 °C restart	Thermal state matters for restart dynamics [7]
Variable-load test range	3,500 A at 1.7 MPa to 1,400 A at 1.7 MPa	Minimum-load transition without pressure change [7]
Extended low-load point	800 A at 0.6 MPa	Illustrates deeper turndown with altered pressure [7]
Characteristic response scales	seconds / minutes / hours	Current / HTO-pressure / temperature dominated [7]
Review-based integration insight	Coupling factor >99%, practical STH efficiency around 10%	Battery support can improve operation but raises cost [6]

Taken together, these literature-reported experiments explain why a ramp-rate-limited, storage-buffered strategy is more credible than a pure renewable-following schedule.

In the present model, the battery absorbs fast renewable excursions so that the electrolyzer set-point remains within a slower operating envelope. This interpretation is consistent with the experimental hierarchy of time constants reported in [7] and with the review evidence that slower variables, such as temperature and pressure, become the limiting factors during variable operation [6].

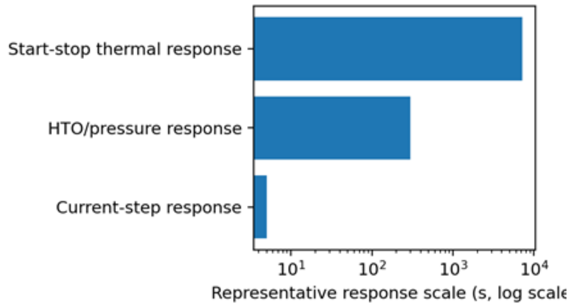

Fig. 6. Literature-reported response-scale hierarchy for industrial water electrolysis.

Fast electrical response coexists with slower gas-quality, pressure, and thermal transients, motivating ramp-limited supervisory control.

The benchmark data also sharpen the interpretation of the storage-sensitivity results. In the reference simulations, the main gain appears when battery capacity increases into the 0.8–1.2 MWh range. This should not be read as a universal plant-sizing result, but as an operational threshold above which the storage can meaningfully reshape sub-hour renewable disturbances before they propagate into minute-scale gas-quality and pressure constraints or hour-scale thermal penalties. Therefore, the reported improvement in resilience is supported both by the simulation results and by the dynamic limitations observed experimentally in industrial electrolysis systems [6]–[8].

VIII. DISCUSSION

The results demonstrate that the secure and resilient operation of a modular power-to-liquid plant depends on the coordinated behaviour of the hybrid PV-wind-storage supply system, not only on the nominal efficiency of the conversion chain. By combining deterministic supervisory optimization with battery buffering, disturbance-aware evaluation, sensitivity analysis, Monte Carlo uncertainty modelling, electrolyzer ramp constraints, and a degradation-aware operating index, the study shows that resilience, system stability, and disturbance handling can be materially improved through integrated system design.

A practical next step is hardware-in-the-loop validation. The control logic proposed in this paper is lightweight enough to be implemented in a MATLAB/Simulink supervisory layer or in an industrial PLC environment. A test bench that emulates renewable power, battery exchange, and electrolyzer constraints would make it possible to verify whether the simulated resilience gains remain visible when measurement delays, actuator saturation, and safety interlocks are introduced. Such a validation pathway would directly connect the conference contribution to future secure-energy demonstrators.

A second limitation is that the degradation-aware index used here is intentionally compact. It is suitable for dispatch-level comparison because it captures the penalties associated with ramps, start-stop events, and near-limit operation, but it does not replace stack-specific aging coefficients obtained from long-duration laboratory campaigns. Future work should therefore combine supervisory scheduling with experimentally calibrated degradation parameters, especially for PEM systems exposed to frequent renewable cycling [5], [8].

The present work remains a reduced-order operational study rather than a full plant digital twin. The hydrogen-production block and the aggregate fuel-synthesis block are intentionally simplified for supervisory-control analysis. The reported trends are therefore most reliable for short disturbances and day-scale scheduling. For longer multi-hour shortages, seasonal renewable asymmetry, or forecast-based dispatch, the relative value of hydrogen buffering, day-ahead planning, and reserve management would likely increase. These effects should be explored in future work by coupling the present supervisory layer to longer-horizon forecasts and seasonally resolved renewable traces.

IX. LIMITATIONS AND FUTURE WORK

The present work remains a reduced-order operational study rather than a full plant digital twin. The hydrogen-production block and the aggregate fuel-synthesis block are intentionally simplified for supervisory-control analysis, and the hydrogen buffer is represented through continuity metrics rather than through an explicit mass-balance trajectory. Consequently, the reported trends are most reliable for short disturbances and day-scale scheduling, while longer shortages require explicit hydrogen-buffer dynamics, synthesis demand constraints, and buffer-depletion risk assessment.

A second limitation concerns uncertainty modelling. The Monte Carlo ensemble uses synthetic amplitude perturbations to test control robustness, but it does not reproduce site-specific solar irradiance, wind-speed correlation, seasonal asymmetry, forecast bias, or multi-day weather persistence. Future work should therefore replace the synthetic renewable traces with measured or reanalysis-based profiles and should evaluate day-ahead or model-predictive dispatch under forecast uncertainty.

A third limitation is the uncalibrated nature of the degradation index. The index is useful for comparing dispatch strategies because it penalizes ramps, restarts, and near-limit operation, but it should be validated against stack-specific aging measurements before being used for maintenance planning or lifetime prediction. A practical validation roadmap should include a 30–60 min renewable-drop ride-through test, start-stop cycling measurements, variable-load gas-quality and pressure monitoring, and battery-buffering tests that record state-of-charge swing, curtailed energy, and dispatched-power smoothness.

These limitations do not invalidate the control-oriented conclusions; rather, they define the boundary between a reduced-order supervisory study and the next stage of experimental and digital-twin validation.

X. CONCLUSION

The overall conclusion of this work is that modular e-fuel production under disturbed renewable input must be designed and operated as a coupled secure energy-conversion system. Within the adopted reduced-order supervisory formulation, the optimized strategy improves modelled fuel continuity, reduces electrolyzer-power variance, and enhances the disturbance-window resilience score relative to the no-buffer baseline. At the same time, the study shows that renewable-mix selection, battery sizing, and supervisory-control logic must be co-designed if secure and resilient operation is to be achieved under realistic renewable fluctuations. The main contribution is therefore methodological: a disturbance-aware, storage-buffered, degradation-conscious supervisory framework that is suitable for future extension toward higher-fidelity plant models and experimental validation.

ACKNOWLEDGMENT

This scientific report is funded by the Ministry of Education and Science in implementation of the Scientific Program „Security and Defence“, adopted by Decree No. 731 of 21.10.2021 and pursuant to Agreement No. D01-74/19.05.2022.

REFERENCES

[1] A. Savachkin, W.Ardila-Rueda, D. Romero-Rodriguez, K. Hua, J.N.D.L. Cruz, Assessment and Optimization of System Resilience: A Critical Review. In: Borowik, G., Chmaj, G., Waszkowski, R. (eds) Models and Methods for Systems Engineering. Studies in Big Data, 2025, vol 165. Springer, Cham. https://doi.org/10.1007/978-3-031-76440-0_20.

[2] INERATEC, "ERA ONE – e-Fuels made in Germany," 2026. [Online]. Available: https://www.ineratec.de/en/era-one-e-fuels-made-germany. [Accessed April 17, 2026].

[3] INERATEC, "INERATEC opens ERA ONE: Europe's largest e-Fuel production plant goes into operation in Frankfurt," Jun. 3, 2025. [Online]. Available: https://www.ineratec.de/en/news/ineratec-opens-era-one-europes-largest-e-fuel-production-plant-goes-operation-frankfurt. [Accessed April 17, 2026].

[4] IEA (2025), *Global Hydrogen Review 2025*, IEA, Paris, [Online]. Available: https://www.iea.org/reports/global-hydrogen-review-2025, [Accessed April 17, 2026].

[5] H. Sayed-Ahmed, A. I. Toldy, and A. Santasalo-Aarnio, "Dynamic operation of proton exchange membrane electrolyzers—Critical", Renewable and Sustainable Energy Reviews, Volume 189, Part A, 2024, 113883, ISSN 1364-0321, https://doi.org/10.1016/j.rser.2023.113883.

[6] V. A. Martinez Lopez, H. Ziar, J. W. Haverkort, M. Zeman, and O. Isabella, "Dynamic operation of water electrolyzers: A review for applications in photovoltaic systems integration", Renewable and Sustainable Energy Reviews, 2023, ISSN 1364-0321, https://doi.org/10.1016/j.rser.2023.113407.

[7] J. Gu et al., "Experimental studies on dynamic performance of 250-kW alkaline electrolytic system", Journal of Power Sources, Volume 592, 2024, 233920, ISSN 0378-7753, https://doi.org/10.1016/j.jpowsour.2023.233920.

[8] H. Y. Jung, Y. S. Jun, K.-Y. Lee, H. S. Park, S. K. Cho, and J. H. Jang, "Effect of Ramping Rate on the Durability of Proton Exchange Membrane Water Electrolysis During Dynamic Operation Using Triangular Voltage Cycling", Journal of Electrochemical Science and Technology, vol. 15, no. 2. The Korean Electrochemical Society - English Journal, pp. 253–260, 31-May-2024.

[9] Giedraityte A, Rimkevicius S, Marciukaitis M, Radziukynas V, Bakas R. Hybrid Renewable Energy Systems—A Review of Optimization Approaches and Future Challenges. Applied Sciences. 2025; 15(4):1744. https://doi.org/10.3390/app15041744.

[10] Schmidt, P., Batteiger, V., Roth, A., Weindorf, W. and Raksha, T. (2018), Power-to-Liquids as Renewable Fuel Option for Aviation: A Review. Chemie Ingenieur Technik, 90: 127-140. https://doi.org/10.1002/cite.201700129

[11] C. Huang et al., "The complementary role of E-fuel in decarbonizing transportation and stabilizing the power grid", Renewable and Sustainable Energy Reviews, Volume 224, 2025, 116033, ISSN 1364-0321, https://doi.org/10.1016/j.rser.2025.116033.

[12] V. Dieterich, A. Buttler, A. Hanel, H. Spliethoff and S. Fendt. "Power-to-liquid via synthesis of methanol, DME or Fischer–Tropsch-fuels: a review.", Energy & Environmental Science, 2020, 13, 3207-3252, https://doi.org/10.1039/D0EE01187H.

[13] A. A. Kebede, T. Kalogiannis, J. Van Mierlo, M. Berecibar, "A comprehensive review of stationary energy storage devices for large scale renewable energy sources grid integration", Renewable and Sustainable Energy Reviews, Volume 159, 2022, 112213, ISSN 1364-0321, https://doi.org/10.1016/j.rser.2022.112213.

[14] P. Gabrielli, M. Gazzani, E. Martelli, and M. Mazzotti, "Optimal design of multi-energy systems with seasonal storage", Applied Energy, Volume 219, 2018, Pages 408-424, ISSN 0306-2619, https://doi.org/10.1016/j.apenergy.2017.07.142.

[15] Schmiegel, Armin U., Energy Storage Systems: System Design and Storage Technologies (Oxford, 2023; online edn, Oxford Academic, 22 June 2023), https://doi.org/10.1093/oso/9780192858009.001.0001, [Accessed 17 April, 2026].